Journal of Materials Chemistry C

Accepted Manuscript

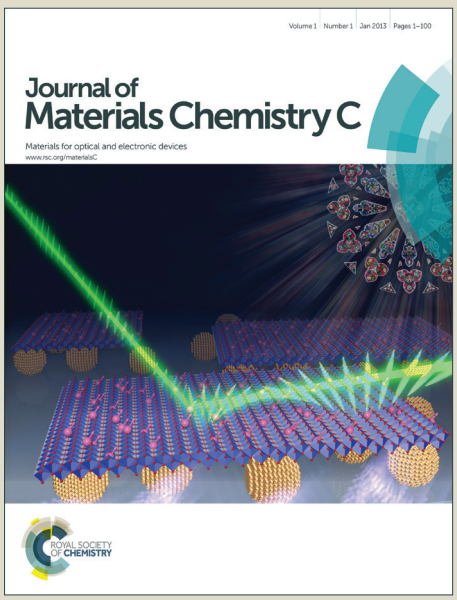

ROYAL SOCIETY OF CHEMISTRY

www.rsc.org/materialsC

Energy and Environmental Science

ARTICLE

Enhancement of the thermoelectric properties of *n*-type PbTe by Na and Cl co-doping

Received 00th January 20xx,
Accepted 00th January 20xx

DOI: 10.1039/x0xx00000x

www.rsc.org/

I. Cohen,[a] M. Kaller,[a] G. Komisarchik,[a] D. Fuks,[a] and Y. Gelbstein[a]

In an attempt to reduce our reliance on fossil fuels, associated with severe environmental effects, the current research is focused on enhancement of the direct thermal to electrical thermoelectric efficiency of *n*-type PbTe by Na and Cl co-doping. We show that such co-doping is expected to enhance the thermoelectric efficiency by more than 17% compared to any of the previously reported lanthanum or iodine doped single-phase compositions, due to reduced lattice thermal conductivity values, originated by lattice disordering and mass/radii fluctuations in addition to improved carrier mobilities, originated by lower effective masses.

Introduction

In recent years demands for energy efficiency have motivated many researchers globe-wide to seek for innovative methods capable of enhancement the efficiency of heat to electricity thermoelectric (TE) energy conversion [1-3]. Since the dimensionless TE figure of merit, ZT ($=\alpha^2 T\rho^{-1}\kappa^{-1}$, where α - Seebeck coefficient, ρ - electrical resistivity, κ - thermal conductivity and T- absolute Temperature), can be regarded as proportional to the TE efficiency for a given temperature difference, materials improvements in this direction include either electronic optimization methods for maximizing the $\alpha^2\rho^{-1}$ product or phonons scattering methods for minimization of the thermal conductivity (the denominator of ZT). These methods and approaches mainly involve interfaces and sub-micron generation methods, which are much more effective in phonon scattering (rather than electron scattering) and consequently reducing the lattice contribution to the thermal conductivity, κ_l, without adversely affecting the other involved electronic properties.

Lead and germanium chalcogenides and their alloys are considered as among the most efficient TE compositions for temperatures of up to ~450°C [4]. While GeTe rich alloys (e.g. $Ge_xPb_{1-x}Te$ [4-6] and $Ge_x(Sn_yPb_{1-y})_{1-x}Te$ [7-8]) exhibit outstanding *p*-type TE properties, due to high intrinsic hole concentrations, PbTe rich alloys are more versatile and can be doped for achieving either *n*- or *p*- type conduction. High ZTs were recently reported upon SrTe [9-10], MgTe [11], PbSe [12] and CdTe [13] alloying of PbTe as *p*-type TE compositions, and PbS [14], Ag_2Te [15-16], La_3Te_4 [17] alloying as *n*-type PbTe rich TE compositions. In all of these compositions in addition to the more complicated *p*-type $Ag_x(Pb,Sn)_mSb_yTe_{2+m}$ (LASTT) [18], $NaPb_mSbTe_{2+m}$ (SALT) [19], and *n*-type $AgPb_mSbTe_{2+m}$ (LAST) [20], KPb_mSbTe_{m+2} (PLAT) [21], PbTe rich alloys, the ZT enhancement was mainly attributed to nano clustering due to phase segregation and/or alloying disordering effects, reducing the lattice thermal conductivity. For electronic fine tuning of the carrier concentration values and thereby controlling the *p*- or *n*- type conductivities, Na or PbI_2 were mostly applied as acceptor or donor atoms, respectively, although other elements such as lanthanum and chlorine as donor elements, are suitable candidates as well. In a simplified way, for the case of iodine, acting as a donor in PbTe, the substitution of I^{-1} for Te^{-2} is equivalent to the addition of a positive charge in the anion site, contributing one free electron to the conduction band, for maintaining electron neutrality. Similarly, the substitution of Na^{+1} for Pb^{+2} is equivalent to the addition of a negative charge in the cation site, contribution one hole to the valence band. Yet, since practically an addition of PbI_2 or Na_2Te molecules into PbTe is more straightforward than the introduction of atomic iodine or sodium, the doping mechanism can be also interpreted differently. In this case, the substitution can be considered as the replacement of two molecules of PbTe by one of PbI_2 or Na_2Te, creating one Pb or Te vacancy, respectively. In case

[a] Department of Materials Engineering, Ben-Gurion University of the Negev, Beer-Sheva, Israel.

that excess Pb or Te atoms are present, they can occupy this vacancy, contributing two free electrons or holes to the conduction or valence band, respectively. The specified above doping mechanisms are very simplified. Practical selection of dopants, for controlling the charge carrier concentrations in semiconductors, is determined not only by their position in the periodic table, but also by the solubility and chemical interaction with the host matrix, volatility, and their interaction with structural defects (e.g. vacancies). For example for the case of solubility of impurity atoms in the cation or anion vacancies, it is clear that the soubility depends on the vacancy concentration in the initial material, which is highly dependent on the exact synthsis approach applied, as well as on the size of the impurity atoms. Therefore a higher solubility of the smaller Cl donor halogen for example, compared to I, in the Te sub-lattice (ionic radii of 181, 206 and 211 pm for the case of Cl^{1-}, I^{1-} and Te^{2-}, respectively [22,23]) of PbTe, might be expected. Regardless the exact solubility limit of Cl in $PbTe_{1-x}Cl_x$, variations of the lattice parameter (investigated by x-ray diffraction, XRD, analysis) upon introduction of Cl atoms in this system, were attributed to the formation of both Pb- and Te- sites vacancies, in the crystal-chemical formula of $Pb_{1-x}(\square_{Pb})_xTe_{1-2x}(\square_{Te})_xCl_x$ [23]. In this case, the Cl donor action was interpreted in terms of reduction of the Te- site vacancies concentration through the surface or dilocations, acting as defect sinks. Recently, *n*-type Pb(Te,Se,S) TE composites were doped with $PbCl_2$ [24] and HCl [25] in order to substitute divalent anions (Te^{2-}, Se^{2-}, S^{2-}) with monovalent Cl^- anions. In these cases Cl was chosen as a dopant instead of iodine due to a better ionic radius matching between sulfur (170 pm) and chlorine (181 pm) compared to iodine (206 pm), in the lead sulfide lattice. Indeed iodine exhibits a better ionic radius matching to Te (211 pm) than chlorine, in PbTe, which might explain it's common acceptance as a donor dopant in PbTe, for the same reason that Cl was chosen as a donor in PbS. Yet, as pointed out above, the exact electronic doping mechanism of PbTe by Cl is still not completely clear and for TE applications, the radii mismatch between Te and Cl (compared to iodine) in addition to the higher mass fluctuations (35.45, 126.90 and 127.60 amu for Cl, I and Te, respectively), might be beneficial for κ_l reduction via phonon scattering. Furthermore, due to the fact that Cl doping was already associated with the formation of cation site vacancies, possible occupation of such vacancies by co-doping with Na^{+1} ions (ionic radius of 102 pm compared to 112 pm for Pb^{2+} [22,23]), for enhancing the donor action (rather than substitution of Pb^{2+} cations for an acceptor action) while Cl is absent, is plausible.

In the current research the doping contribution of Cl and NaCl in PbTe on the TE transport properties was investigated. Impressive *n*-type TE properties were observed for all of the investigated Cl and NaCl doped compositions. A significat enhancement of *ZT* in the temperature range of 100-450°C, compared to any of the the previously published iodine or lanthanum doped PbTe compounds, was obtained upon 0.3% NaCl doping of PbTe, as shown by the red curve in Fig. 1_a.

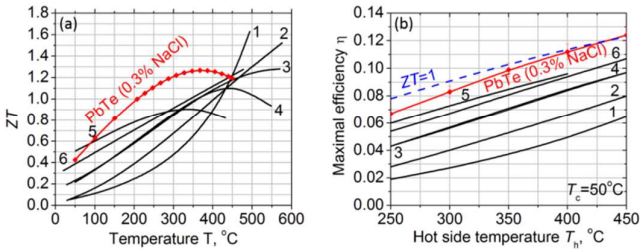

Fig. 1. (a) Temperature dependence of the TE figure of merit, *ZT*, of the currently investigated *n*-type 0.3% NaCl doped PbTe compared to the previously published (1) La-doped PbTe with Ag_2Te nano-precipitates [12], (2) $PbTe_{0.9972}I_{0.0028}$ [26], (3) $Pb_{1-x}La_xTe$ (n=2x10^{19}cm^{-3}) [17], (4) 0.03 mol%PbI_2 doped PbTe [27], (5) 9.104x10^{-3} mol%PbI_2 doped PbTe [27], (6) La-doped $(PbTe)_x(Ag_2Te)_{1-x}$ [16] compositions. (b) Calculated maximal TE efficiency values, η, for the same compositions, using eq. 1, for a constant cold side temperature, T_c, of 50°C and varied hot side temperatures, T_h.

In addition, a broader maximum of the temperature dependence of *ZT* for the currently reported NaCl doped sample, compared to each of the previously reported standard iodine/lanthanum doped compositions, indicating a higher average *ZT* over the investigated temperature range, as required for power generation applications, is clearly visible in this figure. The maximal TE efficiencies associated with each of these composition, shown in Fig. 1_b, were calculated using eq. 1 for a constant cold side temperature, T_c, of 50 °C and varied hot side, T_h, temperatures.

$$\eta = \frac{\Delta T}{T_h} \cdot \frac{\sqrt{1+\overline{ZT}}-1}{\sqrt{1+\overline{ZT}}+\frac{T_c}{T_h}} \quad (1)$$

where, $\overline{ZT}$ - average dimensionless TE figure of merit and ΔT-temperature difference along the TE sample (ΔT=T_h-T_c).

It can be clearly seen from this figure that a maximal TE efficiency of ~12.5% is expected for the currently investigated 0.3% NaCl doped PbTe, while being operated in the 50-450°C temperature range, which is significantly higher compared to each of the previously investigated compositions indicated in the figure. The effect of the ionic radii mismatch between Te (211 pm), Cl (181 pm) in the anion site and Na (102 pm), Pb (112pm) in the cation site, in

addition to the mass fluctuations between these lighter dopants compared to the heavier host Pb and Te atoms, on reduction of the lattice thermal conductivity and optimization of the electronic properties, upon Na and Cl co-doping of PbTe, are described in details.

Experimental

PbTe compositions doped by 0.3 and 0.5 at% Cl, 0.1 and 0.3 mol% NaCl and 3 at% Na were synthesized by arc melting (MAM-1, Edmund Bühler GmbH, Germany) from pure Pb, Te, $PbCl_2$ (Alfa aesar, 99%, for Cl doping), Na_2Te (American Elements, Merelex corp., 99.9% for Na doping) and NaCl (Merck, 99.5%), under argon atmosphere. The 0.3% Cl and NaCl doped and the 3% Na doping levels were optimized for achieving similar absolute room temperature Seebeck coefficient values of ~100μV/K, reflecting a similar carrier concentration level, while the 0.5% Cl and 0.1% NaCl doped samples were selected for understanding the doping action of these constituents in PbTe. The Na doped composition was selected for analysing possible variations of the lattice thermal conductivity due to solely Na doping under the same synthesis route.

Each of the compositions were flipped and re-melted more than five times to ensure homogeneity.

Each synthesized ingot was crushed by a mortar and pestle and filtered through a 60 mesh sieve.

The sieved powder was spark plasma sintered (SPS) (type HP D 5/1 FCT GmbH) under a mechanical pressure of 25MPa at 550°C for 60 minutes, resulting in high density values of >95% of the theoretical density.

The samples' crystal structure and lattice parameters were analysed by X-ray powder diffraction (XRD; Rigaku DMAX 2100 powder diffractometer, scan step of 0.01° in the 20-110° 2Θ range). The measurement error of the lattice parameters was calculated as the variance obtained by calculations based on the four peaks at the highest angles (in the 90-110° range). The microstructural characterizations and the chemical composition analysis were conducted by scanning electron microscopy (HRSEM; JEOL JSM-7400) and electron probe microanalyzer (EPMA), respectively.

Seebeck coefficient, α, and the electrical resistivity, ρ, were measured by Linseis LSR-3/800 Seebeck coefficient / electrical resistance measuring system. The total thermal conductivity, κ, was determined as a function of temperature from room temperature to 450°C using the flash diffusivity method (LFA 457, Netzsch). The front face of a disc-shaped sample (∅=12 mm, thickness≈1-2mm) was irradiated by a short laser burst, and the resulting rear face temperature was recorded and analysed. The total thermal conductivity values were calculated using the equation $\kappa=\gamma \cdot C_P \cdot \xi$, where γ is the thermal diffusivity, C_P is the specific heat (measured using differential scanning calorimetry, STA 449 - Netzsch), and ξ is the bulk density of the sample (calculated from the sample's geometry and its mass). For evaluation of the room temperature carrier concentration and mobility, Hall effect experiments were performed in a home-made apparatus described previously [28], using a permanent magnet of 1 T and electrical currents in the range of 100-200 mA, under a vacuum of 10^{-5} Torr.

Results and discussion

Following SPS all of the synthesized samples were found by HRSEM and XRD as single phase without any noticeable micro-scale dopants precipitation or segregation. Nevertheless, following the first arc-melting stage, the NaCl doped samples, exhibited ~30μm NaCl cubes (Fig. 2_b), with an increased dissolution level in the PbTe matrix, reflected by the decomposition of these cubes into <1μm domains, following the subsequent flipping and re-melting stages (Fig. 2_a) of the arc-melting synthesis, until the appearance of a uni-phase PbTe matrix following the fifth arc-melting re-melting stage.

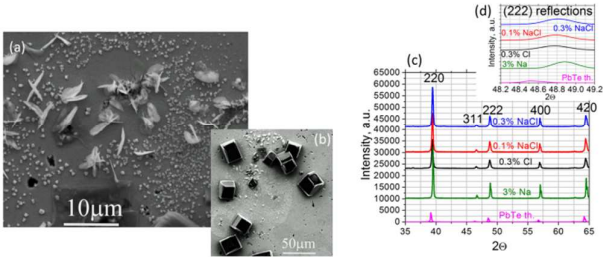

Fig. 2. HRSEM micrographs of the NaCl doped samples, following the 2nd (a) and 1st arc-melting synthesis stages, reflecting ~30μm NaCl cubes, decomposed into finer (~1μm) domains, due to dissolution inside the PbTe matrix. XRD patterns of the entire investigated spectrum (c) and in the vicinity of the (222) reflections (d) following five re-melting stages compared to theoretical PbTe peaks [29].

Such dopant residuals, following the first re-melting stages, were not observed for any of the other Na and Cl doped samples, reflecting a stronger interaction between the Na and Cl ions, in NaCl molecules, compared to the Cl-Pb and Na-Te interactions in the $PbCl_2$ and Na_2Te molecules, applied for the Cl- and Na- doped samples,

respectively. It can be seen from the XRD patterns following five re-melting stages (Fig. 2$_c$), that only PbTe peaks without any reflections from any impurity phases were detected for the investigated Na-, Cl- and NaCl- doped samples, reflecting a complete dissolution of the dopants into the PbTe matrix, without any precipitations. Careful investigation of these diffractograms, reveals a shift of the peak position toward higher angles compared to pure PbTe (Fig. 2$_d$). By combining Bragg's law (eq. 2, left) and the cubic lattices planar spacing, d_{hkl}, dependence of the lattice parameter, a (eq. 2, right), it can be easily seen that the observed higher angles peaks' shift, reflects a reduction trend of the lattice parameter, upon Na-, Cl- and NaCl- doping, compared to pure PbTe (a=6.460Å [29]), as shown in Table 1.

$$n\lambda = 2d_{hkl}sin\theta \qquad d_{hkl} = \frac{a^2}{\sqrt{h^2+k^2+l^2}} \tag{2}$$

where, h,k,l are the Miller indices of the cubic planes being considered.

Table 1. Measured by XRD, a_{meas}, and calculated by eqs. 3-5, a_{calc}, lattice parameters of the investigated alloys (δ designates the reduction amount of the measured compared to the calculated values), as well as room temperature Hall effect measured carrier concentration, n, and carrier mobility, μ, values. The actual dopant concentrations were determined by EPMA.

Alloy	Actual dopant concentration, %	a_{meas}, Å (±0.0006)	a_{calc}, Å	δ, %	n, cm^{-3}	μ, cm^2/Vs
0.1% NaCl	0.07	6.4531	6.4597 (eq. 5)	1.02x10^{-1}	4.9x10^{18} (n)	1563
0.3% NaCl	0.24	6.4528	6.4590 (eq. 5)	9.66x10^{-2}	6.6x10^{18} (n)	1341
0.3% Cl	0.26	6.4541	6.4584 (eq. 3)	6.72x10^{-2}	2.2x10^{19} (n)	1139
0.5% Cl	0.47	6.4550	6.4572 (eq. 3)	3.38x10^{-2}	3.7x10^{19} (n)	1010
3% Na	0.49	6.4539	6.4590 (eq. 4)	7.93x10^{-2}	1.8x10^{19} (p)	121

Since as was discussed in details in the introduction, the ionic radii of chlorine and sodium are smaller than those of tellurium and lead, respectively, the introduction of chlorine or sodium is expected to reduce the lattice parameter of PbTe. As was already reported for the case of $PbTe_{1-x}Cl_x$ solid solutions, chlorine doping of PbTe, just due to substitution of Te^{2-} ions, is expected to exhibit the a values obtained by eq. 3 [23].

$$a(PbTe_{1-x}Cl_x) = 2(r_{Cl^-} - r_{Te^{2-}})x + 2(r_{Pb^{2+}} + r_{Te^{2-}}) = 0.646 - 0.06x\ [nm] \tag{3}$$

where, r_{Cl^-}, $r_{Te^{2-}}$ and $r_{Pb^{2+}}$, represent the ionic radii of Cl^-, Te^{2-} and Pb^{2+}, respectively.

However, as can be seen in Table 1, the measured lattice parameter upon 0.3% Cl doping is 6.72x10^{-2} % lower than the calculated using eq.3, implying on an involvement of another active mechanism such as the formation of vacancies, since the formation of a vacancy causes the neighbouring atoms to displace toward the vacant site, thereby further reducing the lattice parameter.

Adopting the same approach, also for the cases of $Pb_{1-x}Na_xTe$ and $(PbTe)_x(NaCl)_{1-x}$ solid solutions, leads to eqs. 4 and 5, respectively.

$$a(Pb_{1-x}Na_xTe) = 2(r_{Na^+} - r_{Pb^{2+}})x + 2(r_{Pb^{2+}} + r_{Te^{2-}}) = 0.646 - 0.02x\ [nm] \tag{4}$$

where, r_{Na^+} represents the ionic radius of Na^+.

$$a(Pb_{1-x}Na_xTe_{1-x}Cl_x) =$$

$$= 2(r_{Na^+} + r_{Cl^-} - r_{Te^{2-}} - r_{Pb^{2+}})x + 2(r_{Pb^{2+}} + r_{Te^{2-}}) =$$

$$= 0.646 - 0.08x\ [nm] \tag{5}$$

Please note, that the x in eq. 5, represents the atomic fractions of Na and Cl in the cation and anion sub-lattices, respectively, which is half of the molecular fraction of the NaCl dopant agent.

It can be seen in Table 1 that most of the introduced dopant concentrations are in a good agreement with the originally designed nominal values, except of the 3% Na doped alloy, in which a much lower dopant concentration of ~0.49% was observed by EPMA. This fact can be attributed to the lower solubility limit of Na (in the range of ~0.5% [30-31] compared to Cl (in the range of 4% [32]) in PbTe. Therefore a much lower amount of Na than the originally introduced, actually substituted Pb. Since no secondary Na phase was observed by both HRSEM and XRD, it is believed that most of the remaining 2.5% of Na (with the much lower melting temperature of ~97^{o}C compared to the 924^{o}C of PbTe) was spilled out of the matrix during the solidification process while the melt was cooled. Nevertheless, the lower calculated lattice parameters based on Cl and/or Na substitution of Te and Pb, respectively, using eqs. 3-5, than the experimentally measured for all of the examined compositions, might imply on a noticeable vacancies population.

The room temperature Hall effect measurements indicated a p-type conduction for the Na doped sample in contrast to an n-type conduction observed upon both Cl and NaCl doping. From the measured room temperature carrier concentration and mobility of the investigated samples, Table 1, a donor action of both Cl and NaCl on increasing the carrier concentration, accompanied by reduced mobility values due to enhanced carrier scattering, can be clearly observed. The temperature dependence of the transport properties of the investigated samples, Seebeck coefficient, α, electrical

resistivity, ρ, thermal conductivity, κ, and the TE figure of merit, *ZT*, following SPS, are shown in Figs. $3_{a\text{-}d}$, respectively. It can be seen in Fig. 3_a that solely Na doping resulted in positive α values, reflecting a *p*-type conduction in the entire investigated temperature range, while both the solely doped Cl and co-doped NaCl samples exhibited negative α values reflecting an *n*-type conduction, in agreement with Hall effect measurements, Table 1. Increasing the Cl and NaCl dopant concentration from 0.3 to 0.5% and from 0.1 to 0.3%, respectively, resulted in decreased absolute α values (Fig. 3_a) and decreased ρ values (Fig. 3_b), reflecting an electrons donor role for both of these dopants on increasing the total carrier concentration. This trend is also supported by the increased electronic thermal conductivity, κ_e, values with increasing of the Cl and NaCl doping concentrations (increased values of curve 1 compared to curve 2 and of curve 3 compared to curve 4, respectively), shown in the insert of Fig. 3_b. These κ_e ($=L\rho^{-1}T$) values were analyzed using Lorentz constant, *L*, values, calculated from the measured α values (Fig. 3_a) in a procedure described previously [27], the measured electrical resistivity, ρ, values (Fig.3_b) and the absolute temperature, *T*.

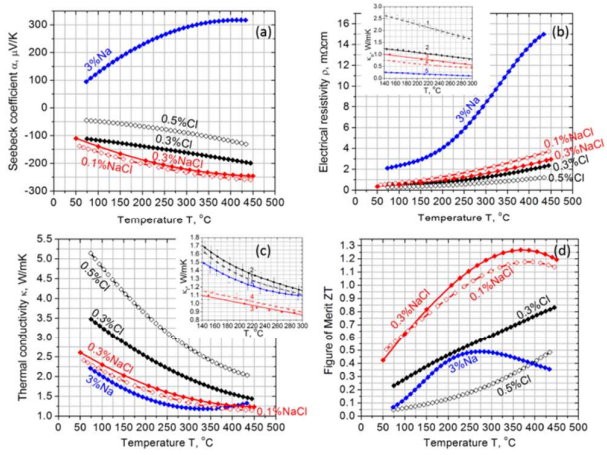

Fig. 3. Temperature dependencies of the TE transport properties, Seebeck coefficient (a), electrical resistivity (b), thermal conductivity (c) and the TE figure of merit (d). Calculated electronic and lattice contributions to the thermal conudctivity, κ_e and κ_l, are shown in the inserts of Figs. 3_b and 3_c, respectively, for the investigated PbTe samples doped by 0.5% Cl (1), 0.3% Cl (2), 0.3% NaCl (3), 0.1% NaCl (4) and 3% Na (5).

For further analysing the electronic effects upon Na, Cl and NaCl doping of PbTe, room temperature Pisarenko plots, based on equations 6-9 [27], were calculated and compared to the experimentally measured α (Fig. 3_a) and *n* (Table 1) values, as can be seen in Fig. 4.

$$\alpha = \frac{k}{e}\left[\frac{\left(\frac{5}{2}+r\right)F_{\frac{3}{2}+r}}{\left(\frac{3}{2}+r\right)F_{\frac{1}{2}+r}} - \eta\right] \quad (6)$$

$$n = \frac{4}{\sqrt{\pi}}\left(\frac{2\pi m^* kT}{h^2}\right)^{3/2} F_{\frac{1}{2}} \quad (7)$$

$$F_r = \int_0^\infty \xi^r f_0(\eta) d\xi \quad (8)$$

$$f_0(\eta) = \frac{1}{1+e^{\xi-\eta}} \quad (9)$$

where, e, k, h, m^*, F_r, η, f_o, r and ξ are the electrons charge, Boltzmann and Planck constants, carrier effective mass, Fermi integral, reduced Fermi potential ($=E_F/kT$), Fermi distribution function, the carrier scattering parameter and the kinetic energy of a charge carrier, respectively.

In this analysis, a scattering parameter, *r*, of -0.5, taking into account scattering of the charge carriers by acoustic phonons, as the dominant scattering mechanism in PbTe based materials [27], was applied.

From Fig. 4, it can be seen that the experimental points obtained upon solely Na and Cl doping (points 1, 2 and 5, respectively) coincide with the Pisarenko curve calculated taking into account a higher effective mass, m^*, of $0.33m_o$, in eq. 2, compared to those obtained upon NaCl doping (points 3 and 4), coinciding with the curve calculated with $m^*=0.23m_o$.

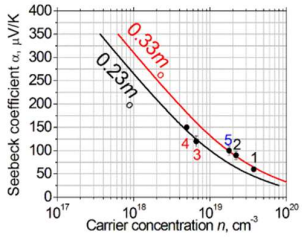

Fig. 4. Calculated room temperature Pisarenko curves, using effective masses of 0.23 and 0.33mo, based on eqs. 6-9, compared to experimental measured values of the investigated PbTe samples doped by 0.5% Cl (1), 0.3% Cl (2), 0.3% NaCl (3), 0.1% NaCl (4) and 3% Na (5). Absolute Seebeck coefficient values are shown.

Although high effective masses are generally associated with enhanced Seebeck coefficient values for any given carrier concentration value, it was recently shown upon lanthanum and iodine doping of PbTe, that under the typical acoustic phonon scattering mechanism of the carriers, applied in PbTe, decreasing the effective mass, increases the carrier mobility significantly enough to compensate the decrease in Seebeck coefficient, leading to a net

increase of the power factor, $\alpha^2\rho^{-1}$ [33]. Therefore, lower effective mass values, as was currently observed upon NaCl doping, compared to solely Na and Cl doping, is beneficial for a high TE performance, which explains the higher measured mobility values upon NaCl doping (Table 1).

The measured total thermal conductivity values, κ, shown in Fig. 3_c, were used for calculating the lattice contribution to the thermal conductivity, κ_l ($=\kappa-\kappa_e$), for all of the investigated samples, shown in the insert of Fig. 3_c. In this figure, more than 20% κ_l reduction was obtained upon NaCl co-doping compared to each of the solely doped Na and Cl samples, exhibiting similar κ_l values to those previously reported for PbTe [12, 26, 34]. Lower κ_l values than the currently reported for the NaCl doped samples (~0.85 W/mK at 300°C) were previously only reported for complicated nano-structured PbTe alloys following phase segregation (e.g. $AgPb_mSbTe_{2+m}$ [20] and KPb_mSbTe_{m+2} [21], exhibiting κ_l~0.3 W/mK at 300°C) or phase separation (e.g. $Pb_xSn_{1-x}Te$-PbS [14], with ~0.5 W/mK at 300°C) reactions. Such a reduction of κ_l upon NaCl co doping of PbTe, without any noticeable sub-micron features, can be attributed to the high mass and radii fluctuations associated with the introduction of the lighter and smaller Na^{+1} and Cl^{-1} ions (than Pb^{+2} and Te^{-2}, respectively) into the PbTe lattice, as was explained in the introduction. The effect of the NaCl molecules decomposition and the dissolution of Na and Cl ions into the PbTe lattice on the electronic and lattice properties of PbTe, leading to the enhanced *ZT*s shown in Fig. 3_d, might also be correlated to the variations between the measured and calculated lattice parameters, discussed above referred to Table 1. In case that the dissolution of Na is mainly governed by the substitution of Pb cations in $Pb_{1-x}Na_xTe$, a replacement of Pb^{2+} by Na^+ is equivalent to the addition of a negative charge in the cation site, contribution one hole to the valence band, leading to the observed *p*- type conduction (positive α values in Fig. 3_a). Upon Cl doping, the reduced carrier mobility values, associated with a higher carrier effective mass, might be related to both of the dissolution mechanisms discussed above. Some of the dissolution of Cl^- might be associated with the substitution of Te^{2-} anions in $PbTe_{1-x}Cl_x$, adding a positive charge in the anion site, contributing one free electron to the conduction band, leading to the observed *n*- type conduction (negative α values in Fig. 3_a). On the other hand, the increased vacancies formation, can be attributed to the replacement of two molecules of PbTe by one of $PbCl_2$, creating one Pb vacancy. In that case, an occupancy of such cation vacancies by additionally introduced Na^+ ions is expected to contribute additional one electron per Na^+ ion to the conduction band, supporting the *n*-type conduction observed. Apparently, the effect of Cl^- substitution of Te^{2-} in addition to the creation of cation vacancies occupied by Na^+ ions, resulting in an *n*-type doping action with increased mobility values is combined with the mass fluctuations effect on κ_l reduction, upon NaCl doping of PbTe. It can be seen in Fig.3_d that a >30% *ZT* enhancement was observed upon NaCl doping compared to each of the Na and Cl solely doped compositions, with a ZT_{max} of ~1.27 observed at 375°C for the 0.3% NaCl doped composition. As was explained related to Fig. 1, this co-doped sample, exhibit a wider temperature dependent *ZT* curve in the vicinity of the ZT_{max} value, than any of the previously reported *n*-type iodine or lanthanum doped PbTe samples, reflecting a ~17% maximal TE efficiency enhancement while being subjected to a temperature difference of 50-450°C compared to the previously reported La-doped $(PbTe)_x(Ag_2Te)_{1-x}$ [16] composition (curve 6) and nearly a 100% enhancement compared to the La-doped PbTe containing Ag_2Te nano-precipitates [15] sample, exhibiting a much higher ZT_{max} of 1.65 at 500°C (curve 1).

Conclusions

In the current research the thermoelectric properties following Na and Cl co-doping of PbTe were investigated and compared to those following solely Na and Cl doping. While Na and Cl, are known acceptor and donor, respectively, in PbTe, Na and Cl co-doping exhibited an *n*-type conduction, which can be explained by a Cl creation of Pb vacancies in the cation site and occupation of these vacancies by excess Na^+ ions, contributing additional electrons to the conduction band. Reduced lattice thermal conductivities, which were associated with large mass and radii fluctuations, and higher carrier mobility values, originated from a reduced effective mass, were obtained upon Na and Cl co-doping, enhancing by more than 30% the thermoelectric figure of merit, compared to that obtained following Na and Cl doping separately. The 0.3% NaCl doped composition exhibit a maximal *ZT* of ~1.27 (at 375°C) and a wider temperature dependent *ZT* curve, correspondint to a more than 17% maximal thermoelectric efficiency enhancement, compared to any of the previously reported single phase *n*-type iodine or lanthanum doped PbTe samples, while being operated at a temperature range of 50-450°C, commonly applied in practical applications.

Acknowledgements

The work was supported by the Israel Science Foundation (ISF), Grant nos. 497/12 and 1578/12. The authors would like to thank Mr. Yair George for the synthesis of the alloys and specimen preparation.

1. Sumeet Walia, Rodney Weber, Sivacarendran Balendhran, David Yao, Joel T. Abrahamson, Serge Zhuiykov, Madhu Bhaskaran, Sharath Sriram, Michael S. Strano and Kourosh Kakantar-zadeh, *Chem. Commun.* **48** 7462-7464 (2012).
2. Sumeet Walia, Rodney Weber, Sharath Sriram, Mahu Bhaskaran, Kay Latham, Serge Zhuiykov and Kourosh Kalantar-zadech, *Energy Environ. Sci.* **4** 3558 (2011).
3. Sumeet Walia, Sivacarendran Balendhran, Pyshar Yi, David Yao, Serge Zhuiykov, Muthu Pannirselvam, Rodney Weber, Michael S. Strano, Madhu Bhaskaran, Sharath Sriram and Kourosh Kalantar-zadeh, *J. Phys. Chem. C* **117** 9137-9142 (2013).
4. Yaniv Gelbstein, Joseph Davidow, Steven N. Girard, Duck Young Chung, and Mercouri Kanatzidis, *Advanced Energy Materials* **3** 815-820 (2013).
5. Yaniv Gelbstein, Zinovi Dashevsky, Moshe P. Dariel, *Phys. Stat. Sol.* (RRL) **1**(6) 232-234 (2007).
6. Yaniv Gelbstein, Boaz Dado, Ohad Ben-Yehuda, Yatir Sadia, Zinovy Dashevsky and Moshe P. Dariel, *Journal of Electronic Materials*, **39** (9), 2049 (2010).
7. Yaniv Gelbstein, Yoav Rosenberg, Yatir Sadia and Moshe P. Dariel, *Journal of Physical Chemistry* C, **114**, 13126-13131 (2010).
8. Y. Rosenberg, Y. Gelbstein and M.P. Dariel, *Journal of Alloys and Compounds*, **526**, 31-38 (2012).
9. Kanishka Biswas, Jiaqing He, Ivan D. Blum, Chun-I-Wu, Timothy P. Hogan, David N. Seidman, Vinayak P. Dravid and Mercouri Kanatzidis, *Nature* **489** 414 (2012).
10. Kanishka Biswas, Jiaqing He, Qichun Zhang, Guoyu Wang, Ctirad Uher, Vinayak P. Dravid and Mercouri G. Kanatzidis, *Nature Chemistry* **3** 160 (2011).
11. Michihiro Ohta, Kanishka Biswas, Shih-Han Lo, Jiaqing He, Duck Young Chung, Vinayak P. Dravid and Mercouri G. Kanatazidis, *Adv. Energy Mater.* **2** 1117-1123 (2012).
12. Yanzhong Pei, Xiaoya Shi, Aaron LaLonde, Heng Wang, Lidong Chen and G. Jeffrey Snyder, *Nature* **473** 66 (2011).
13. Yanzhong Pei, Aaron D. LaLonde, Nicholas A. Heinz and G. Jeffrey Snyder, *Adv. Energy Mater.* **2** 670-675 (2012).
14. John Androulakis, Chia-Her Lin, Hun-Jin Kong, Ctirad Uher, Chun-I Wu,Timothy Hogan, Bruce A. Cook, Thierry Caillat, Konstantinos M. Paraskevopoulos and Mercouri G. Kanatzidis, *J. Am. Chem. Soc.* **129** 9780-9788 (2007).
15. Yanzhong Pei, Jessica Lensch-Falk, Eric S. Toberer, Douglas L. Medlin and G. Jeffrey Snyder, *Adv. Funct. Mater.* **21** 241-249 (2011).
16. Yanzhong Pei, Andrew F. May and G. Jeffrey Snyder, *Adv. Energy Mater.* **1** 291-296 (2011).
17. Yanzhong Pei, Zachary M. Gibbs, Andrei Gloskovskii, Benjamin Balke, Wolfgang G. Zeier and G. Jeffrey Snyder, *Adv. Energy Mater.* **4** 1400486 (2014).
18. John Androulakis, Kuei Fang Hsu, Robert Pcionek, Huijun Kong, Ctirad Uher, Jonathan J. D'Angelo, Adam Downey, Tim Hogan, and Mercouri G. Kanatzidis, *Adv. Mater.* **18** 1170–1173 (2006). (LASTT)
19. Pierre F. P. Poudeu, Jonathan D'Angelo, Adam D. Downey, Jarrod L. Short, Timothy P. Hogan and Mercouri G. Kanatzidis, *Angew. Chem. Int. Ed.* 45 3835 –3839 (2006). (SALT)
20. Kuei Fang Hsu, Sim Loo, Fu Guo, Wei Chen, Jeffrey S. Dyck, Ctirad Uher, Tim Hogan, E. K. Polychroniadis, Mercouri G. Kanatzidis, *Science* **303** 818 (2004).
21. Pierre F. P. Poudeu, Aurelie Gueguen, Chun-I Wu,Tim Hogan, and Mercouri G. Kanatzidis, *Chem. Mater.* **22** 1046–1053 (2010).
22. R.D. Shannon, *Acta Cryst.* **A32** 751 (1976).
23. M.K. Sharov, O.B. Yatsenko and Ya. A. Ugai, *Inorganic Materials* **43**(2) 132-134 (2007).
24. Sima Aminorroaya Yamini, Heng Wang, Dianta Ginting, David R.G. Mitchell, Shi Xue Dou and G. Jeffrey Snyder, *Appl. Mater. Interfaces* **6** 11476-11483 (2014).
25. Maria Ibanez, Rachel J. Korkosz, Zhishan Luo, Pau Riba, Doris Cadavid, Silvia Ortega, Andreu Cabot and Mercouri G. Kanatzidis, accepted to *J. Am. Chem. Soc.* (2015).
26. Aaron D. LaLonde, Yanzhong Pei and G. Jeffrey Snyder, *Energy Environ. Sci.,* **4** 2090 (2011).
27. Y. Gelbstein, Z. Dashevsky and M.P. Dariel, *Physica B* **363** 196-205 (2005).
28. O. Appel and Y. Gelbstein, *Journal of Electronic Materials* **43**(6) 1976 (2014).
29. A. Ishida, M. Aoki, H. Fujiyasu, *J. Appl. Phys.* **58** 797-801 (1985).

30. Jiaquing He, Li-Dong Zhao, Jin-Cheng Zheng, Jeff W. Doak, Haijun Wu, Hui-Qiong Wang, Yeseul Lee, Chris Wolverton, Mercouri G. Kanatzidis and Vinayak P. Dravid, *J. Am. Chem. Soc.* **135** 4624-4627 (2013).
31. Hongchao Wang, Junphil Hwang, Matthew Loren Snedaker, Il-ho Kim, Chanyoung Kang, Jungwon Kim, Galen D. Stucky, John Bowers and Woochul Kim, *Chem. Mater.* **27** 944-949 (2015).
32. M.K. Sharov, O.B. Yatsenko and Ya. A. Ugai, *Inorganic Materials* **42**(7) 723-725 (2006).
33. Yanzhong Pei, Aaron D. LaLonde, Heng Wang and G. Jeffrey Snyder, *Energy Environ. Sci.* **5** 7963-7969 (2012).
34. Mercouri G. Kanatzidis, *Chem. Mater.* **22** 648-659 (2010).